Supporting Information

(9 pages, 7 figures)

A Single-Emitter Gain Medium for Coherent Radiation from a Plasmonic Nanoresonator

Pu Zhang[1], Igor Protsenko[2], Vahid Sandoghdar[3], and Xue-Wen Chen[1*]

[1]School of Physics, Huazhong University of Science and Technology, Luoyu Road 1037, Wuhan, 430074, People's Republic of China

[2]Lebedev Physical Institute, Leninsky prospect 53, Moscow, 119991, Russia

[3]Max Planck Institute for the Science of Light, Staudtstr. 2, D-91058 Erlangen, Germany

[*]Email: xuewen_chen@hust.edu.cn

1. Electromagnetic simulation of the optical antenna

Here we present the optical properties of the antenna obtained from electromagnetic simulation. By taking advantage of the rotational symmetry of the antenna structure, we use the rigorous and computationally efficient body of revolution finite-difference time-domain (BOR-FDTD) method with convolutional perfectly matched layer absorbing boundary condition[1,2] to simulate the electromagnetic response of the antenna. Due to the high efficiency of the BOR-FDTD, extreme fine grid (e.g. 0.1 nm) can be used to ensure the accuracy of the results even for plasmonic structures with highly confined field distribution. The dielectric function of gold is described by a Drude-Lorentzian dispersion model via fitting the tabulated dielectric constants from CRC Handbook of Chemistry and Physics.[3] The refractive index of silica substrate is set to be 1.5.
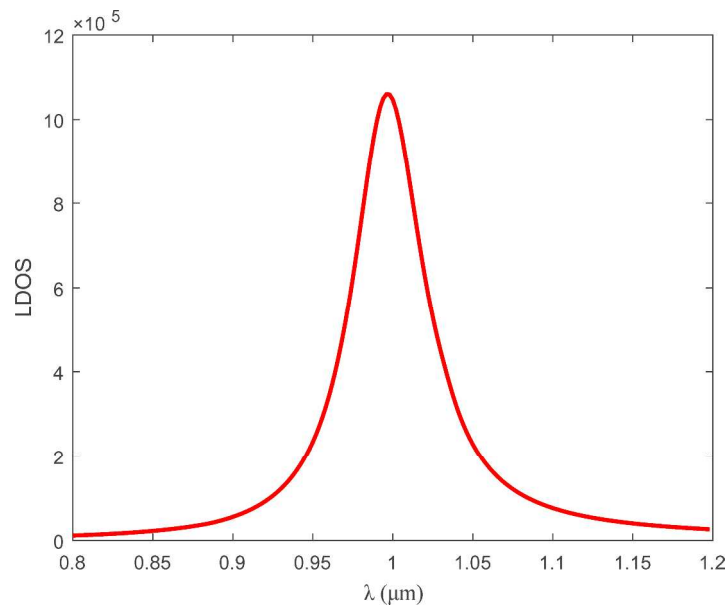

Figure S1 The LDOS spectrum of the antenna with a gap size of 5 nm

Figure S1 shows the spectrum of the normalized localized density of states (LDOS) for an emitter placed in the middle of 5 nm gap for the antenna structure. To obtain the LDOS, we excite the antenna with an electric dipole at the gap center with the orientation along the rotation axis and calculate the total radiated Poynting power. The normalized LDOS is obtained by normalizing the total power in the presence of the antenna with the radiation power in vacuum. The radiation efficiency 53% is calculated as the ratio of the radiated power of the far field to the total radiated power. This radiation efficiency doesn't change appreciably by changing the gap size for the antenna structure. The LDOS spectrum can

be well fitted by a Lorentzian function with a resonant wavelength of 1 μm and a linewidth of 40 meV. Therefore the LDOS spectrum is like the response from a single harmonic oscillator.
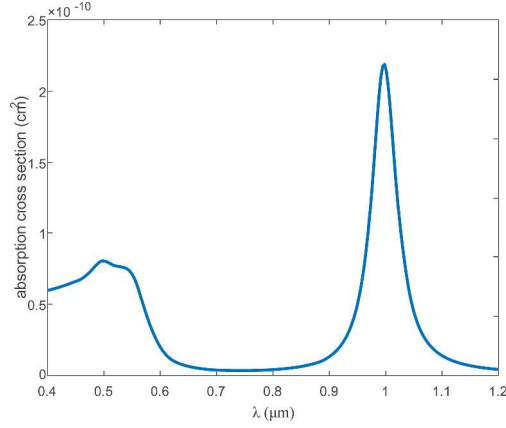

Figure S2 Absorption cross section spectrum of the optical antenna.

Figure S2 displays the spectrum of the absorption cross section (ACS) covering the range from blue to near infrared. To calculate the ACS, we excite the antenna system with a radially polarized beam with an incident angle of 45 degree and compute the absorbed power by the metal and normalize it with the average intensity. One observes that the plasmonic resonance appears as the dominant feature in the absorption cross section spectrum. At the blue end of the spectrum, the absorption exhibits some peaks and bumps instead of monotonously decreasing due to interband absorption of gold.

2. Estimation of the temperature rise

Absorption of the pump lasers generates heat and may cause considerable temperature rise. The heating problem is particularly severe in the blue part of the spectrum, i.e., for the pump at transition $|1> - |3>$, as gold is very absorptive due to interband transitions. Here we explicitly estimate the temperature rise caused by the pump Ω_{13}. We use Rabi frequency to characterize the pump rate. For the Rabi frequency Ω_{13} in the order of 10κ and the dipole moment $\mu = 0.31$ e*nm (corresponding to 1 ns lifetime at the photon energy of 3.0 eV), we have the complex amplitude E_c of the electric field at the gap center

$$E_c = \frac{\hbar\Omega_{13}}{2\mu} = 3.2 \times 10^8 V/m,$$

where we have assumed the electric field is expressed as $E_c(t) = E_c \cos(\omega t - kx) = \frac{1}{2} E_c \left[e^{i(\omega t - kx)} + e^{-i(\omega t - kx)} \right]$. The required light intensity at the position of the emitter is $I_0 = 54 \mathrm{GW}/cm^2$, which is quite intense but still well below the threshold of ionization of atoms and molecules. For ionization, the typical required light intensity is in the order of 10^{13} W/cm^2.[4,5]

The antenna structure provides a factor of 2.9 field enhancement for the incident pump field at the position of the emitter ($E_0 = E_c/2.9$). Thus the incident light intensity turns out to be $I_0 = \frac{1}{2} cn\varepsilon_0 E_0^2 = 8.79 \mathrm{GW}/cm^2$.

The upper limit of the temperature rise can be estimated by using the following formula[6,7]:

$$\delta T_{NP}^0 = \frac{\sigma I_0 \tau}{\beta V \rho_{Au} C_{Au}}$$

where β is a geometrical factor with the value of about 1.2 for the metallic bases, $\rho_{Au} = 19.32$ g/cm^3, C_{Au} = 0.129 J/(g*ºC), the volume of the metallic parts V = 4.92×10^{-15} cm^3. $\sigma = 5.93 \times 10^{-11}$ cm^2 from the absorption cross section spectrum and the pulse duration τ = 1 ps. In the end, we obtain the upper limit of temperature rise $\delta T_{NP}^0 \approx 35.4$ ºC for 1 ps pulse duration or 354 ºC for 10 ps.

3. Time evolution of nanoplasmon number

According to Eq.(2) in the main text, we can calculate the time evolutions of various quantities and as an example we show the time traces of average nanoplasmon number for various pumping parameters.
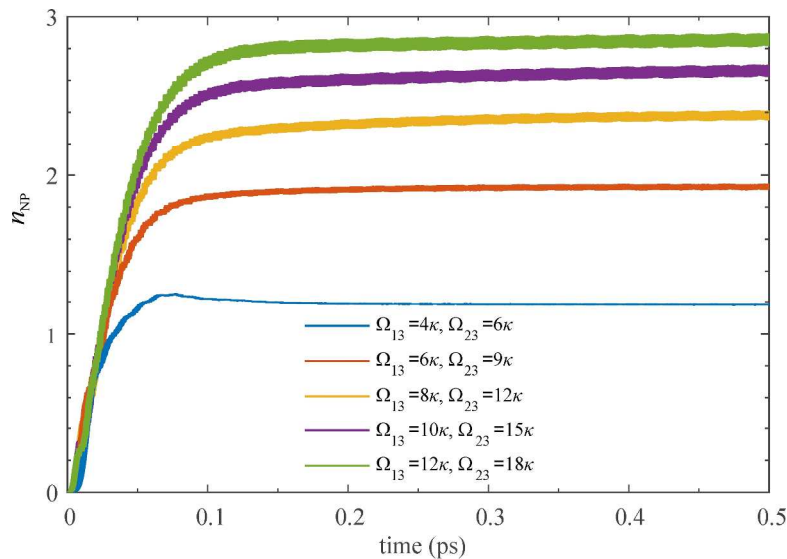
Figure S3 The time traces for average nanoplasmon number for pump rates indicated in the figure.

The pump parameters were chosen on the white-dashed line in Figure 2 of the main text. Our theoretical model is beyond the commonly used rotating wave approximation (RWA) and takes the effects of counter-rotating coupling into account. Therefore, one sees from the time traces that the solution at long time (t>0.2 ps) consists of a steady-state component and fast oscillations with a small amplitude, which is due to the counter rotating couplings and grows as the pump rates increase. For the pump rates considered in the main text, the amplitudes of the fast oscillations are within 2% of the steady-state value and can be averaged out.

4. Second-order intensity correlation $g^{(2)}(\tau)$

We calculate the time delayed second-order intensity correlation function for four pairs of typical pump parameters (corresponding to Figure 2d-2g in the main text) and show the results in Figure 4S.
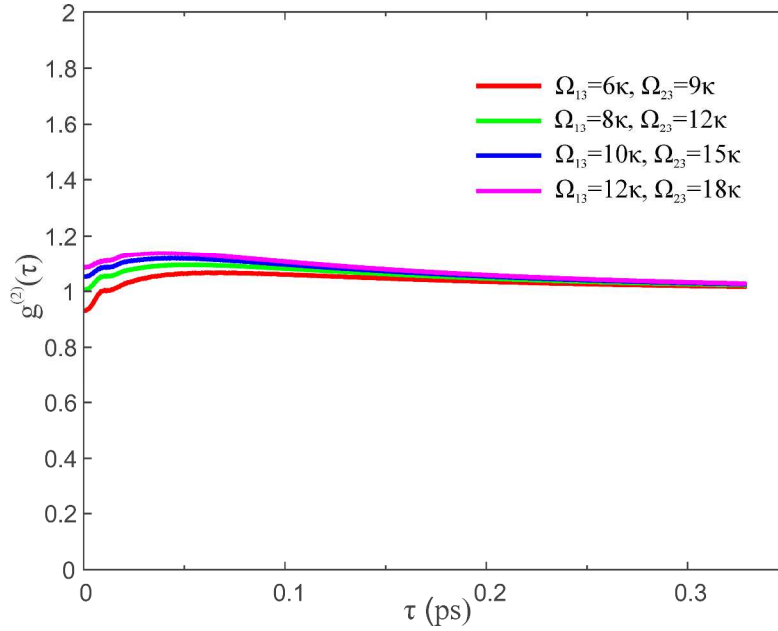

Figure S4 Second-order intensity correlation function v.s. time delay

The correlation functions are not perfectly one at all time but the deviation from 1 is quite small for all the time. The deviation decays towards zero within very short time (within 0.2 ps). These observations further confirm that the nanoplasmon emission from the nanoscopic light source is nearly coherent.

5. Atomic population inversions of the emitter for the nanoscopic coherent light source

The population difference (inversion) between $|2\rangle$ and $|1\rangle$ are plotted in Figure S5 for $g = 100$ meV at pumps along the white-dashed line ($\Omega_{23}=1.5\Omega_{13}=1.5\Omega$) in Figure 2 of the main text and for smaller coupling constants at equal pump $\Omega_{23}=\Omega_{13}=\Omega$. The average nanoplasmon numbers n_{NP} are also displayed as blue-solid lines in Figure S5. Note that there are two vertical axes, i.e., the left one is for the atomic inversion and the right one is for n_{NP}. From these plots, one sees that for all the coupling constants n_{NP} increases from zero to a considerable value before the population inversion turns to be positive. For g=100 meV, on the white dashed line in Figure 2 of the main text, the population inversion stays negative in the whole pump range under consideration. We also observe local maxima in nanoplasmon number for $g = 5$, 10 and 20 meV when the inversion crosses zero. At larger pumps the inversion slowly falls below zero due to counter rotating coupling, but the nanoplasmon number keeps growing towards saturation.
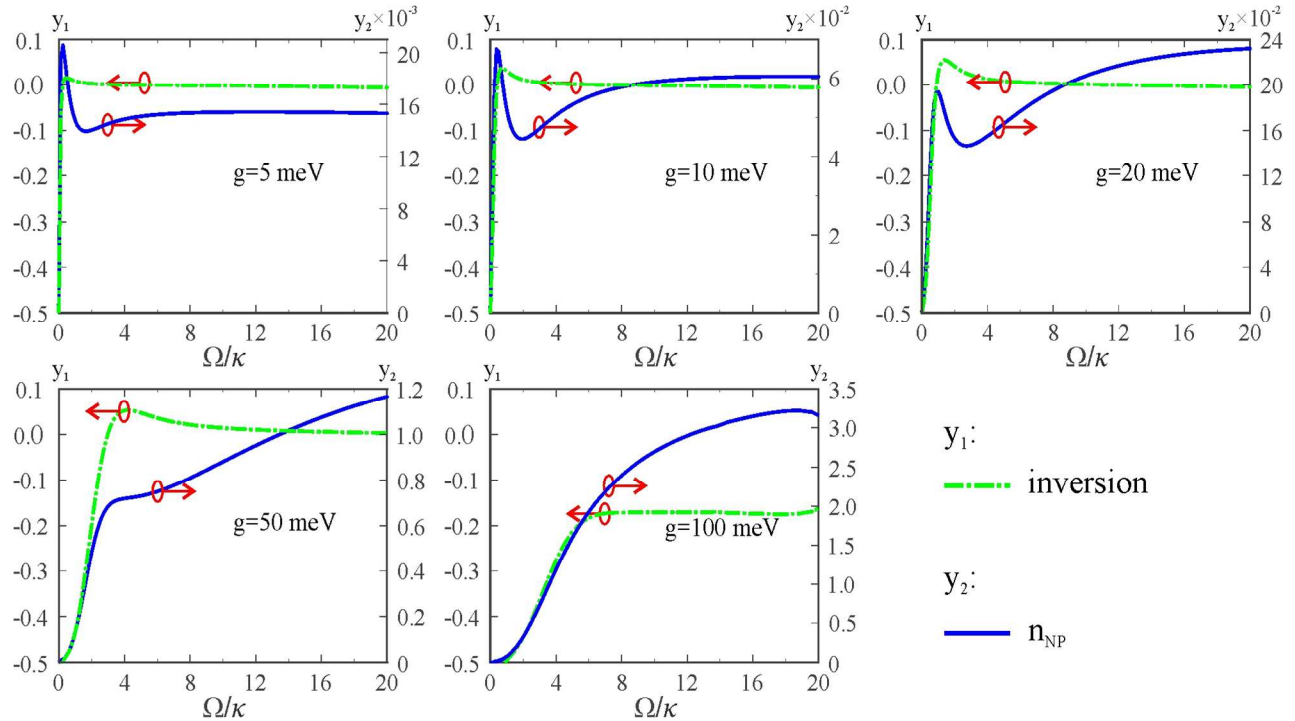

Figure S5 The evolution of atomic population inversion and nanoplasmon number as functions of the pump rate Ω for various coupling constants.

6. Dephasing effect in the weak coupling regime

The effects of fast dephasing on the average nanoplasmon number and the zero time delay second-order intensity correlation function $g^{(2)}(0)$ are studied in the weak coupling regime, in particular the case of g = 10 meV, and the results are summarized in Figure S6. The contours of $g^{(2)}(0)$ from 0.95 to 1.05 are overlaid on the color maps of average nanoplasmon number. It can be seen that in the weak coupling regime the nanoscopic light source is still robust against fast dephasing. The average nanoplasmon number is only weakly affected and coherent emission can always be achieved at proper pump rates.
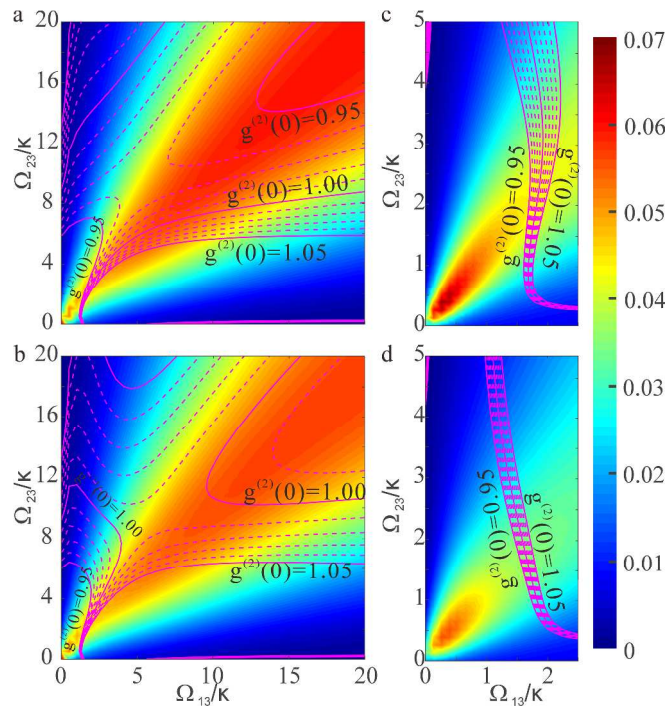

Figure S6 Average nanoplasmon number and second-order intensity correlation function at zero delay $g^{(2)}(0)$ for g = 10 meV and dephasing rates of 10 GHz (**a**), 100 GHz (**b**), 1 THz (**c**) and 10 THz (**d**). The contours of $g^{(2)}(0)$ = 0.95 to 1.05 are overlaid on the graphs.

7. Rate equation model

A rate equation model is developed to provide a more intuitive understanding of the working mechanism of the nanoscopic light source. Rate equation model is well-known as a good approximation for problems where coherent effects are not important.[8] In our nanoscopic light source, the coherence in

the pumps and built up by stimulated emission is intrinsically beyond the simple rate equation model. However, a coherent pump can be viewed as a bidirectional incoherent pump,[9] and thus a rate equation model may give a qualitative description at least for weak coupling scenarios. The rate equations for the electronic level occupation (n_1, n_2 and n_3) and nanoplasmon number (n_{NP}) read:

$$\frac{dn_{NP}}{dt} = F\left(n_2 - n_1\right)n_{NP} + Fn_2 - \kappa n_{NP}$$

$$\frac{dn_2}{dt} = \Omega_{23}n_3 - \Omega_{23}n_2 - F\left(n_2 - n_1\right)n_{NP} + \gamma_3 n_3 - \left(F + \gamma_e\right)n_2$$

$$\frac{dn_3}{dt} = \Omega_{13}n_1 - \Omega_{13}n_3 + \Omega_{23}n_2 - \Omega_{23}n_3 - \gamma_3 n_3$$

$$n_1 + n_2 + n_3 = 1$$

where $F = 4g^2/\left(\gamma_e + \kappa\right)$. The equation system can be analytically solved, but instead of explicitly giving the lengthy expressions we show in Figure S7 the stationary nanoplasmon number for a case of a small coupling constant g = 10 meV. We can see the rate equation model correctly predicts the general behavior of n_{NP} versus the two pump rates: more nanoplasmons are generated with balanced pump rates, the nanoplasmon number increases with the pump rates thresholdlessly and saturates at large pump rates. Even the saturated value of 0.08 is rather a good approximation of 0.63 according to Figure 3a in the main text.
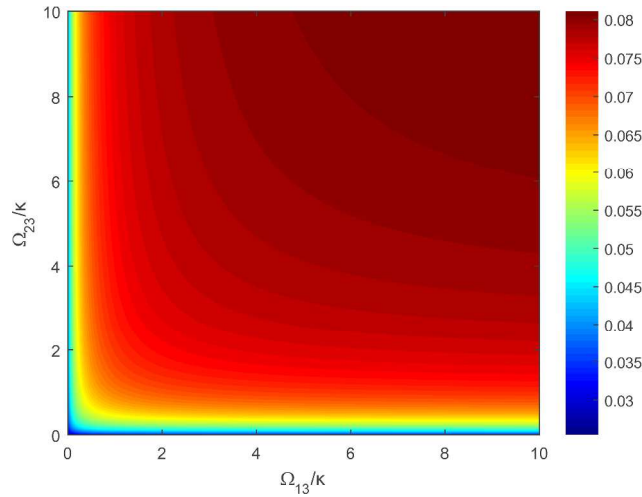

Figure S7 The average nanoplasmon number based on the rate equation model as a function of the pump rates for a weak coupling case (g = 10 meV).

References

(1) Taflove, A.; Hagness, S. C. Computational electrodynamics: the finite-difference time-domain method, 3rd ed.; Artech: Boston, 2005.

(2) Chen, X.-W.; Sandoghdar, V.; Agio, M. Highly Efficient Interfacing of Guided Plasmons and Photons in Nanowires. *Nano Lett.* **2009**, 9, 3756–3761.

(3) Haynes, W. CRC Handbook of Chemistry and Physics, 87th ed.; Haynes, W., Eds.; CRC Press/Taylor and Francis Group, LLC: Boca Raton, FL, 2006.

(4) DeWitt M. J. *et al.*, *Phys. Rev. Lett.* **2001,** 87, 153001

(5) Tong X. -M. *et al.*, *Phys. Rev. A* **2002,** 66, 033402.

(6) Baffou, G.; Quidant, R. Thermo-Plasmonics: using metallic nanostructures as nano-sources of heat. *Laser Photon. Rev.* **2013**, 7, 171–187.

(7) Baffou, G.; Quidant, R.; García de Abajo, F. J. Nanoscale Control of Optical Heating in Complex Plasmonic Systems. *ACS Nano* **2010**, 4, 709–716.

(8) Moelbjerg, A.; Kaer, P.; Lorke, M.; Tromborg, B.; Mørk, J. Dynamical properties of nanolasers based on few discrete emitters. *IEEE J. Sel. Top. Quantum Electron.* **2013**, 49, 945-954.

(9) Chusseau, L.; Arnaud, J.; Philippe, F. Rate-equation approach to atomic-laser light statistics. *Phys. Rev. A* **2002**, 66, 053818.